Available online at www.sciencedirect.com
ScienceDirect
Ceramics International 35 (2009) 363–368
CERAMICS INTERNATIONAL
www.elsevier.com/locate/ceramint

Effect of Fe_2O_3 addition on consolidation and properties of 8 mol% yttria-stabilized zirconia by high-frequency induction heated sintering (HFIHS)

In-Jin Shon *, In Kyoon Jeong, Jeong-Hwan Park, Byung-Ryang Kim, Ki-Tae Lee

Department of Advanced Materials Engineering, The Research Center of Advanced Materials Development, Chonbuk National University, 664-14 Duckjin-Dong Duckjin-Gu, Chonju, Chonbuk 561-756, Republic of Korea

Received 1 October 2007; received in revised form 10 October 2007; accepted 6 November 2007
Available online 8 December 2007

Abstract

Dense nanophase 8 mol% yttria-stabilized zirconia was sintered by high-frequency induction heated sintering (HFIHS) within 6 min from 8YSZ nanopowder prepared by co-precipitation method. Sintering was accomplished under the combined effects of an induced current and mechanical pressure. Highly dense 8YSZ with relative density of up to 96% was produced under simultaneous application of a 60-MPa pressure and the induced current. The effects of Fe_2O_3 additions on the sintering behavior, mechanical properties and ionic conductivities of the 8YSZ were investigated.

Keywords: C. Mechanical properties; C. Ionic conductivity; High-frequency induction heated sintering; 8YSZ

1. Introduction

Solid oxide fuel cells (SOFCs) have exceptional potential for use in electric power generation systems because of their high energy conversion efficiency, which can reach up to 65%. In addition, SOFCs have many advantages such as multi-fuel capabilities (hydrogen, carbon monoxide, methane, etc.), simplicity of system design and very low emission of pollutants. 8 mol% yttria-stabilized zirconia (8YSZ) has been extensively used as an electrolyte on SOFCs from the standpoint of its high oxygen-ion and low electronic conductivity at high temperatures and relatively economical cost [1,2].

Nanostructured materials have been widely investigated because they display a wide functional diversity and exhibit enhanced or different properties compared with bulk materials [3]. Particularly, in the case of nanostructured ceramics, the presence of a large fraction of grain boundaries can lead to unusual or better mechanical, electrical, optical, sensing, magnetic, and biomedical properties [4–9]. Nanocrystalline powders have been developed by co-precipitation, the thermochemical and thermomechanical process called spray conversion process (SCP) and high energy milling [10,11]. However, grain size in sintered materials becomes much larger than that in pre-sintered powders due to a fast grain growth during conventional sintering process. Therefore, even though the initial particle size is less than 100 nm, the grain size increases rapidly up to 500 nm or larger during the conventional sintering [12]. So, controlling grain growth during sintering is one of the keys to the commercial success of nanostructured materials. In this regard, high-frequency induction heated sintering (HFIHS) method has been shown to be effective in achieving this goal [13]. And it has been reported that some transition metal oxides, such as MnO_2, Fe_2O_3 and Co_3O_4, are very effective sintering aids for densification of ceria-based samples [14,15].

In this work, we report results on the fabrication of nano-sized 8YSZ powders and sintering of nanostructured 8YSZ material with addition of Fe_2O_3 by high-frequency induction heated sintering, a method, which combines induced current with high-pressure application. The effect of Fe_2O_3 on the mechanical properties and ionic conductivity of 8YSZ electrolyte has been also investigated.

* Corresponding author. Tel.: +82 63 270 2381; fax: +82 63 270 2386.
E-mail address: ijshon@chonbuk.ac.kr (I.-J. Shon).

0272-8842/$34.00
doi:10.1016/j.ceramint.2007.11.006

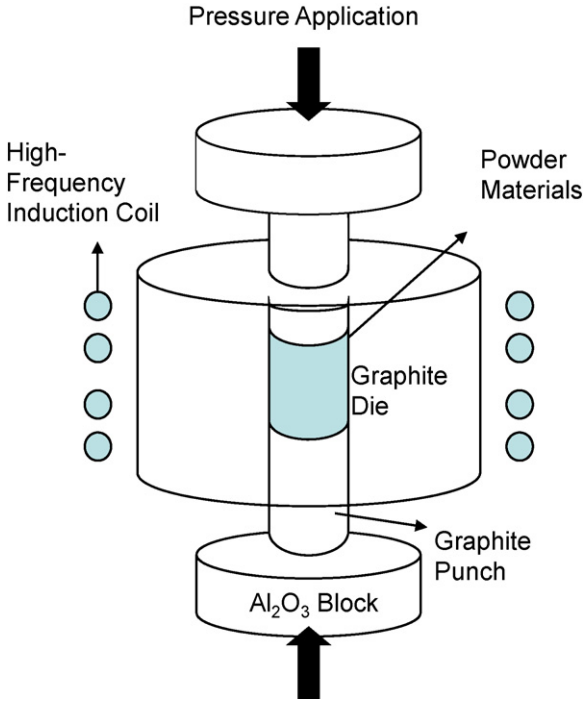

Fig. 1. Schematic diagram of apparatus for high-frequency induction heated sintering.

2. Experimental procedure

Nanopowders of 8YSZ and Fe_2O_3 were made by co-precipitation method using diluted ammonia as precipitant. High purity (>99.9%) reagents $Y(NO_3)_3{\cdot}6H_2O$, $ZrO(NO_3)_2{\cdot}6H_2O$ and $Fe(NO_3)_3{\cdot}9H_2O$ were used as starting materials. 8YSZ and Fe_2O_3 powders were milled in an Universal mill with a ball-to-powder weight ratio of 6:1. Milling was done in polyethylene bottles using zirconia balls and was performed at a horizontal rotation velocity of 250 rpm for 24 h.

The powder was placed in a graphite die (outside diameter, 45 mm; inside diameter, 20 mm; height, 40 mm) and then introduced into the induced current activated sintering system made by Eltek in South Korea, shown schematically in Fig. 1. The HFIHS apparatus includes a 15-kW power supply with 50 kHz frequency and 50 kN uniaxial press. The system was first evacuated and a uniaxial pressure of 60 MPa was applied. An induced current was then activated. Sample shrinkage was measured in real time by a linear gauge measuring the vertical displacement. Temperatures were measured by a pyrometer focused on the surface of the graphite die. Depending on heating rate, electrical and thermal conductivities of the compact and on its relative density, a difference in temperature between the surface and the center of the sample exists. The sample was sintered at 1210 °C temperature with heating rate of 200 °C/min. At the end of the process, the current was turn off and the sample was allowed to cool to room temperature. The process was carried out under a vacuum of 40 mTorr.

Relative densities of the synthesized sample were measured by the Archimedes method. Microstructural information was obtained from fracture surface of product samples. Compositional and microstructural analyses of the products were made using X-ray diffraction (XRD), scanning electron microscopy (SEM) with energy dispersive X-ray analysis (EDAX) and field-emission scanning electron microscopy (FE-SEM). Vickers hardness was measured by performing indentations at load of 1 kgf and a dwell time of 15 s on the samples. After the sintered pellets were polished with SiC paper, silver wires were used as the electrodes and Pt was coated on the both sides of the sintered pellets. Ionic conductivity was measured over 300–400 °C in air using a two-probe impedance spectroscopy (Zahner IM6, Germany) in the frequency range of 100 mHz to 3 MHz with an excitation voltage of 50 mV.

3. Results and discussion

3.1. Powder characterization

Fig. 2 shows FE-SEM image and TEM image of the precipitated 8YSZ powder calcined at 600 °C for 1 h in air.

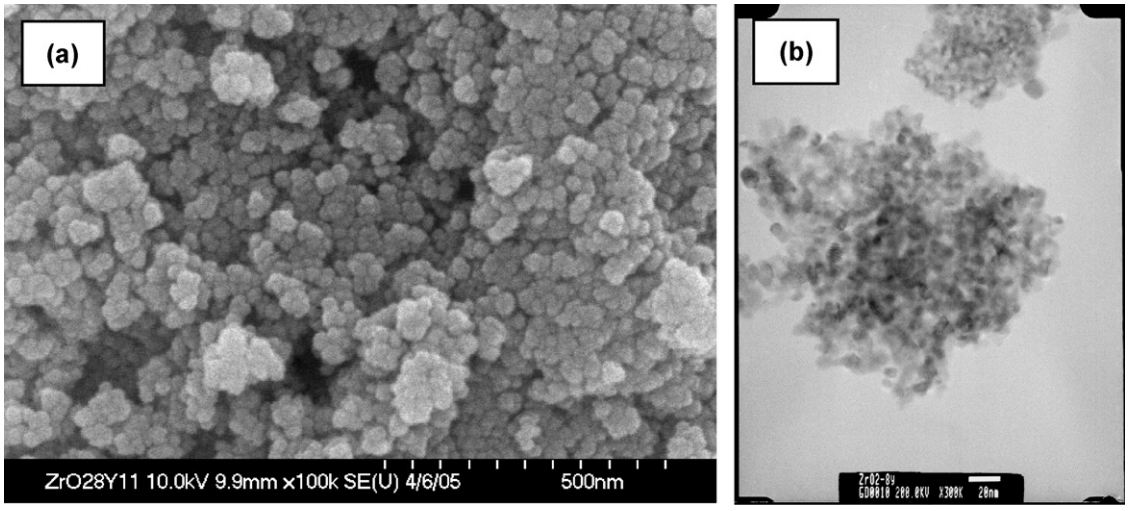

Fig. 2. FE-SEM image (a) and TEM image (b) of the 8YSZ powder made by co-precipitation method.

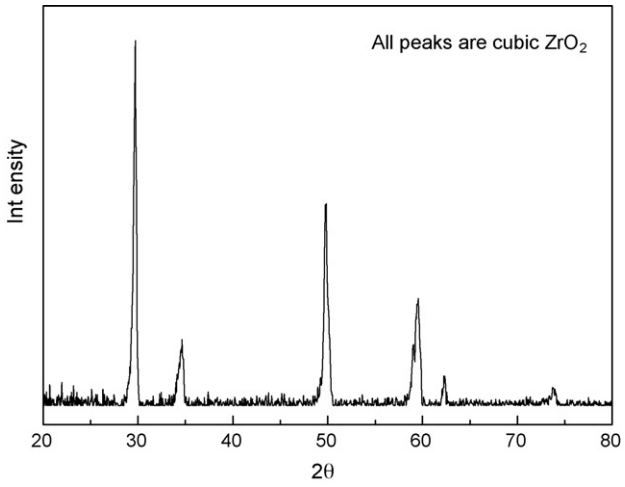

Fig. 3. XRD result of the 8YSZ powder made by co-precipitation method.

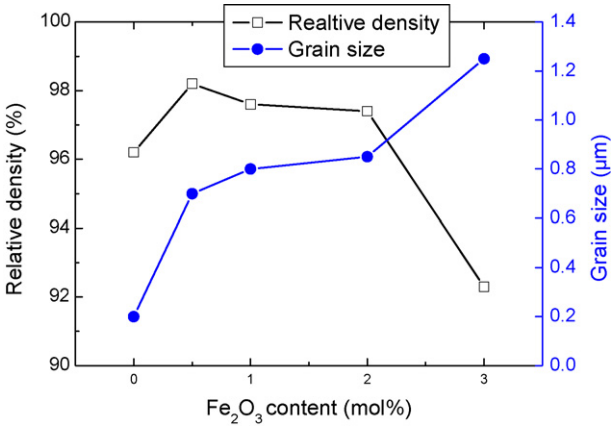

Fig. 5. Relative densities and grain sizes of the 8YSZ as a function of Fe_2O_3 contents.

XRD results (Fig. 3) showed that all the peaks of the powder calcined at 600 °C corresponded to the fluorite structure of ZrO_2.

The grain size and the internal stress are calculated by Stokes and Wilson's formula [16]:

$$b = b_d + b_e = \frac{k\lambda}{(d\cos\theta) + 4\varepsilon\tan\theta} \quad (1)$$

where b is the full width at half-maximum (FWHM) of the diffraction peak after instrument correction; b_d and b_e are FWHM caused by small grain size and internal stress, respectively; k is constant about 0.9; λ is wavelength of the X-ray radiation; d and ε are grain size and internal stress, respectively; θ is the Bragg angle. b and b_s follow Cauchy form with the relationship: $B_0 = b + b_s$, where B_0 and b_s are FWHM of broadened Bragg peaks and the standard sample's Bragg peaks, respectively. The average grain size 8YSZ measured by Stoke–Wilson equation was about 20 nm.

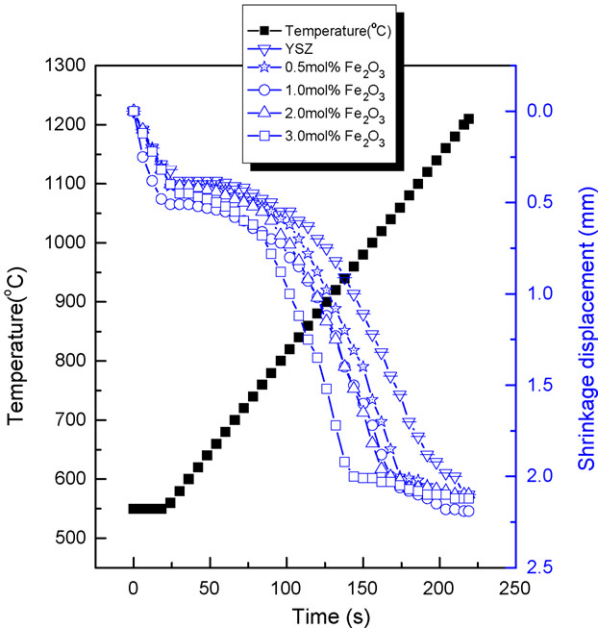

Fig. 4. Variation of temperature and shrinkage displacement of Fe_2O_3 added the 8YSZ with heating time during HFIHS.

3.2. Densification behavior of the 8YSZ oxides

The variations in shrinkage displacement and temperature of the surface of the graphite die with heating time during the processing of 8YSZ doped with different concentration of Fe_2O_3 under 60 MPa pressure are shown in Fig. 4. As the induced current was applied, the shrinkage displacement increased with temperature and Fe_2O_3 doping is extremely effective in promoting the densification of 8YSZ when exceeding a dopant concentration of 0.5 mol%. Fig. 5 shows the density and grain size of 8YSZ as a function of Fe_2O_3 content when the sample was sintered at 1210 °C with a heating rate of 200 °C/min under pressure of 60 MPa. Grain size increased with addition of Fe_2O_3 and relative density increased with increasing Fe_2O_3 content up to 0.5 mol% and then decreased with further addition of Fe_2O_3. As can be seen from Fig. 6, the average size of grains determined by linear intercept method were about 200 nm, 700 nm, 800 nm, 850 nm and 1250 nm for 8YSZ with addition of 0 mol%, 0.5 mol%, 1 mol%, 2 mol% and 3 mol% produced by HFIHS at 1210 °C, respectively.

Fig. 7 shows XRD patterns of the specimens with different Fe_2O_3 contents. The shifts were shown with Fe_2O_3 addition. The lattice constants were calculated from XRD patterns as a function of Fe_2O_3 content, as shown in Fig. 8. The lattice constant decreased with increasing Fe_2O_3 content. This decrease is believed to the substitution of smaller Fe^{3+} ions for Zr^{4+} in the ZrO_2 structure. In line with the above-mentioned explanation for the variation in lattice constant, there is a possibility that Fe_2O_3 additions within the solubility limit induce the substitution of Fe^{3+} ions for Zr^{4+} ions. The addition of Fe_2O_3 in a ZrO_2 system would lead to the formation of oxygen vacancies because of charge compensation. It is expected that these oxygen vacancies enhance the densification rate and promote the grain boundary mobility. Moreover, the

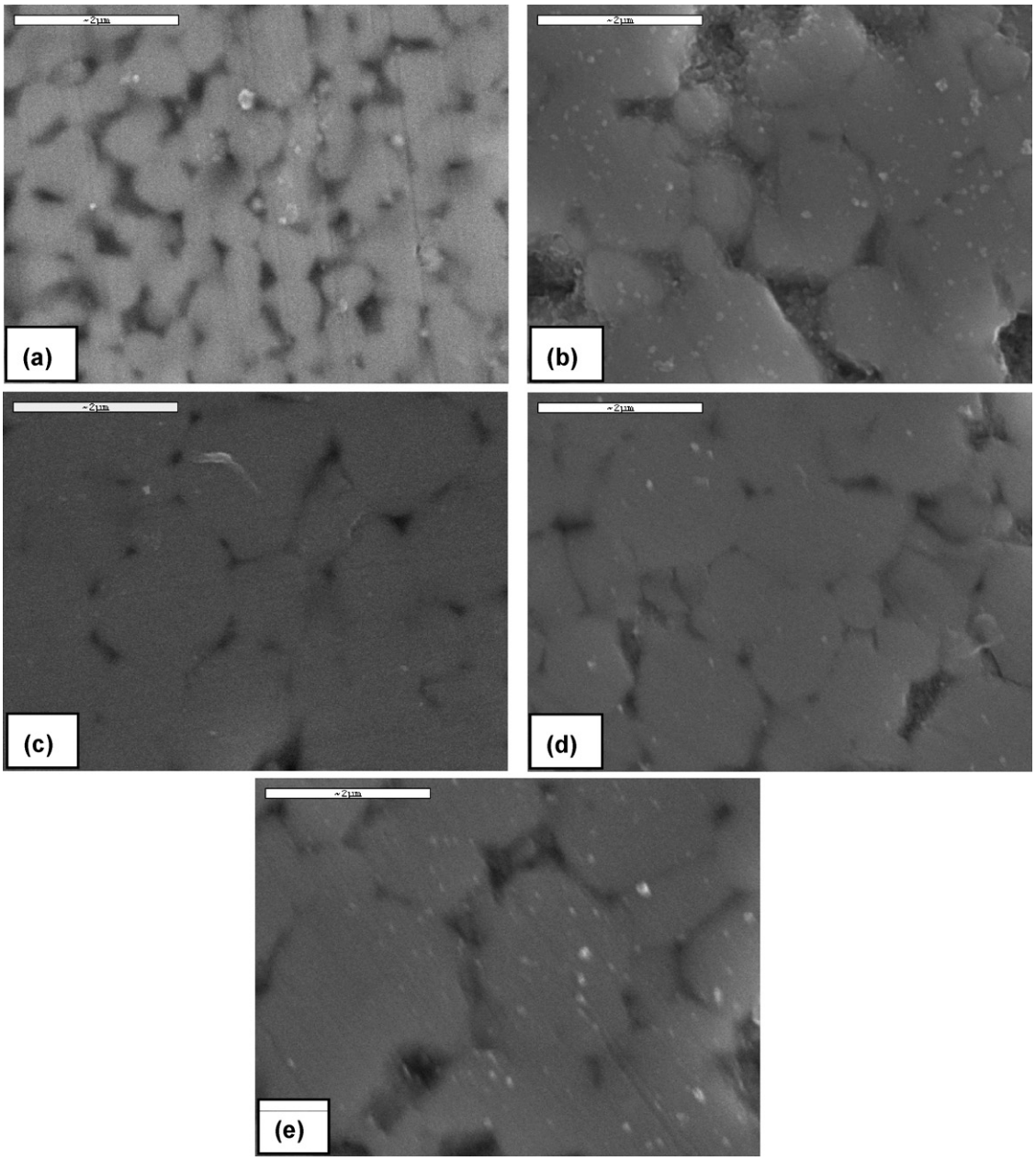

Fig. 6. SEM images of the thermally etched 8YSZ with different Fe_2O_3 contents: (a) 0 mol%, (b) 0.5 mol%, (c) 1 mol%, (d) 2 mol% and (e) 3 mol%.

addition of Fe_2O_3 may induce the large distortion of the surrounding lattice because Fe^{3+} ion has much smaller size compared with that of Zr^{4+} ion. It is also expected that the lattice distortion promotes the grain boundary mobility due to the effect of severely undersized dopant [17].

3.3. Mechanical properties of 8YSZ oxides

To investigate the mechanical properties, Vickers hardness and fracture toughness measurements were made on polished sections of the 8YSZ ceramics using a 1-kgf load and 15 s dwell time. The mechanical properties were investigated on samples densified under 60 MPa with a heating rate of 200 °C/min at 1210 °C. Indentation with large enough loads produced radial cracks emanating from the corners of the indent. Fracture toughness was calculated from cracks produced in indentations under large loads. The length of these cracks permits an estimation of the fracture toughness of the materials by means of the expression [18,19]:

$$K_{IC} = 0.204\left(\frac{c}{a}\right)^{-3/2} H_v a^{1/2} \quad (2)$$

where c is the trace length of the crack measured from the center of the indentation, a is the half of average length of two indent diagonals, and H_v is the hardness.

The results are shown in Fig. 9. There is no great difference in fracture toughness with Fe_2O_3 contents. But the hardness

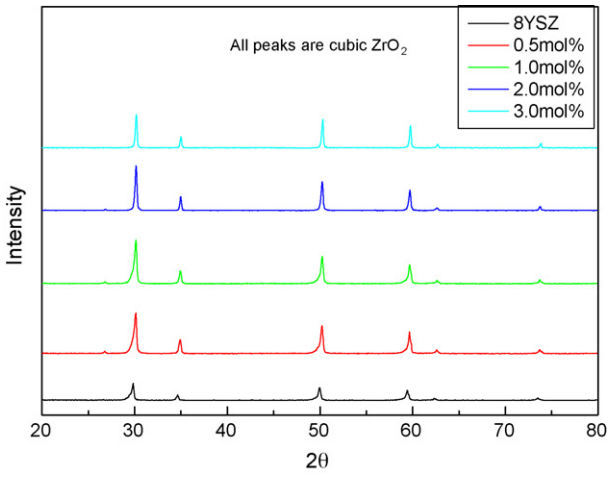

Fig. 7. X-ray diffraction of the sintered 8YSZ with different Fe_2O_3 contents.

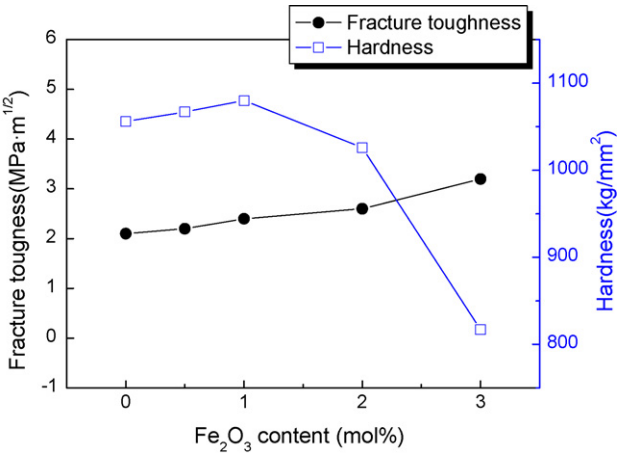

Fig. 9. Variation of hardness and fracture toughness of the 8YSZ as a function of Fe_2O_3 contents.

gradually increased with the addition of Fe_2O_3 up to 1 mol% and then decreased with further addition of Fe_2O_3 due to relative density. The hardness and fracture toughness of 8YSZ sintered at 1210 °C is about 1056 kg/mm^2 and 2.2 MPa m$^{1/2}$, respectively.

3.4. Ionic conductivity of 8YSZ oxides

Figs. 10 and 11 show bulk conductivity and grain boundary conductivity of 8YSZ and 8YSZ with addition of 0.5 mol% Fe_2O_3. The grain boundary conductivity is less than one order of magnitude smaller than the bulk conductivity. In prior studies, it had been assumed that grain boundary resistance is the result of a siliceous phase [20], but more recent observations on samples with impurity-free grain boundaries show that the grain boundary resistance is still about two orders of magnitude higher than the bulk one [21]. In more recent investigation, it has been suggested that oxygen vacancy depletion is effected by dopant ion segregation [22]. There is no great difference in grain interior conductivity and grain boundary conductivity of $Ce_{0.8}Gd_{0.2}O_{2-\delta}$ with addition of Fe_2O_3. The ionic conductivity has been fitted as a function of temperature (T) following the

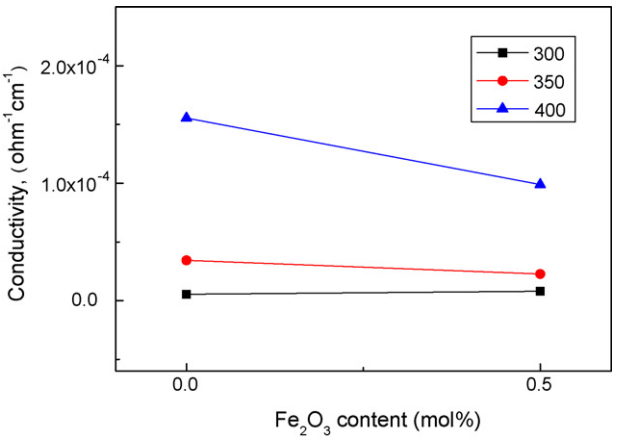

Fig. 10. Variation of grain boundary conductivity of 8YSZ and 8YSZ with addition of 0.5 mol% Fe_2O_3 contents.

Arrhenius law:

$$\sigma = \frac{\sigma_0}{T} \exp\left(-\frac{E_a}{k_B T}\right) \quad (3)$$

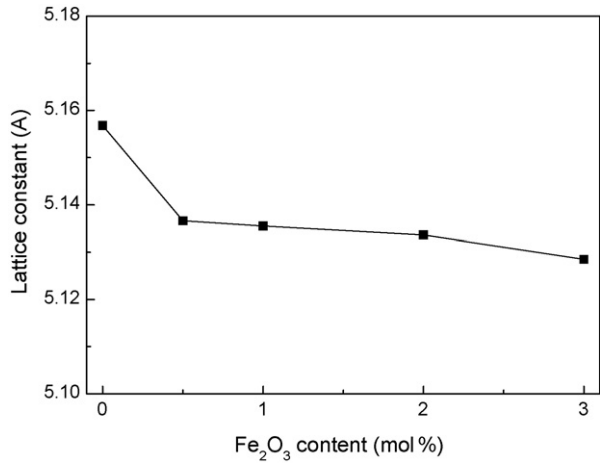

Fig. 8. Lattice constant of 8YSZ as a function of Fe_2O_3 contents.

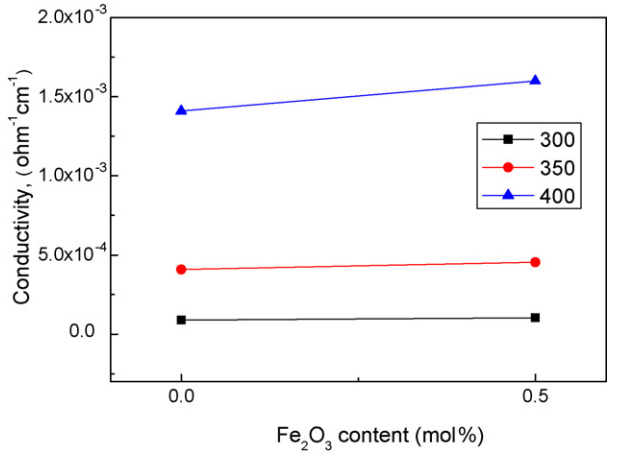

Fig. 11. Variation of grain interior conductivity of 8YSZ and 8YSZ with addition of 0.5 mol% Fe_2O_3 contents.

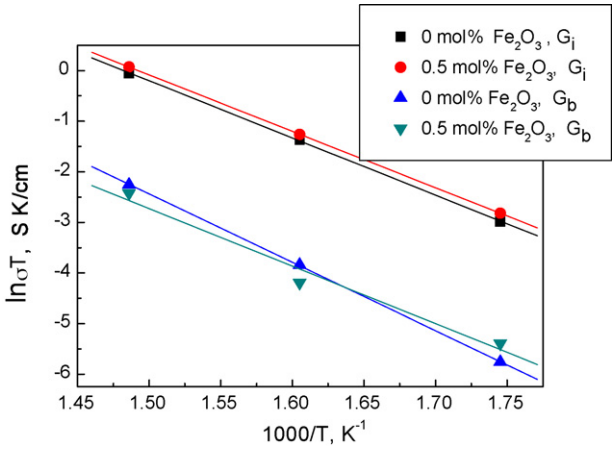

Fig. 12. Arrhenius plot of grain interior (G_i) conductivity and grain boundary (G_b) conductivity of the 8YSZ and 8YSZ with addition of 0.5 mol% Fe_2O_3 contents.

where E_a is the activation energy for ionic migration, k_B is the Boltzmann constant, and σ_0 the pre-exponential factor is a constant related to the density of charge carrier (in this case, oxide vacancies). Fig. 12 shows Arrhenius plots of bulk conductivity and grain boundary conductivity of 8YSZ and 8YSZ with 0.5 mol% Fe_2O_3 contents, respectively. As shown in Figs. 11 and 12, there is no great difference in activation energy with Fe_2O_3 contents. The activation energies of bulk and grain boundary of 8YSZ calculated from Eq. (3) are 0.98 eV and 1.17 eV, respectively.

4. Summary

Using high-frequency induction heated sintering, the densification of nanostructured 8YSZ was accomplished from nanopowder of 8YSZ. The relative density of the 8YSZ was 96% for the applied pressure of 60 MPa and the induced current. Relative density increased with increasing Fe_2O_3 content up to 0.5 mol% and then decreased with further addition of Fe_2O_3 but grain size increased with increasing Fe_2O_3 content. There is no great difference in bulk conductivity and grain boundary conductivity of 8YSZ and 8YSZ with addition of 0.5 mol% Fe_2O_3. The grain boundary conductivity is smaller than the grain bulk conductivity. The activation energies of grain interior and grain boundary of 8YSZ are 0.98 eV and 1.17 eV, respectively. The hardness and fracture toughness of 8YSZ sintered at 1210 °C is about 1056 kg/mm^2 and 2.2 MPa m$^{1/2}$, respectively. There is no great difference in fracture toughness with Fe_2O_3 contents.

References

[1] J. Maier, Nano-sized mixed conductors (aspects of nano-ionics. Part III), Solid State Ionics 148 (2002) 367–374.
[2] J. Schoonman, Nanoionics, Solid State Ionics 157 (2003) 319–326.
[3] H. Gleiter, Nanostructured materials: state of the art and perspectives, Nanostruct. Mater. 6 (1995) 3–14.
[4] J. Karch, R. Birringer, H. Gleiter, Ceramics ductile at low temperature, Nature 330 (1987) 556–558.
[5] A.M. George, J. Iniguez, L. Bellaiche, Anomalous properties in ferroelectrics induced by atomic ordering, Nature 413 (2001) 54–57.
[6] D. Hreniak, W. Strek, Synthesis and optical properties of Nd^{3+}-doped $Y_3Al_5O_{12}$ nanoceramics, J. Alloys Compd. 341 (2002) 183–186.
[7] C. Xu, J. Tamaki, N. Miura, N. Yamazoe, Grain size effects on gas sensitivity of porous SnO_2-based elements, Sens. Actuator B 3 (1991) 147–155.
[8] D.G. Lamas, A. Caneiro, D. Niebieskikwiat, R.D. Sanchez, D. Garcia, B. Alascio, Transport and magnetic properties of nanocrystalline $La_{2/3}Sr_{1/3}MnO_3$ powders synthesized by a nitrate–citrate gel-combustion process, J. Magn. Magn. Mater. 241 (2002) 207–213.
[9] E.S. Ahn, N.J. Gleason, A. Nakahira, J.Y. Ying, Nanostructure processing of hydroxyapatite-based bioceramics, Nano Lett. 1 (2001) 149–153.
[10] Z. Fang, J.W. Eason, Study of nanostructured WC–Co composites, Int. J. Refract. Met. Hard Mater. 13 (1995) 297–303.
[11] A.I.Y. Tok, L.H. Luo, F.Y.C. Boey, Carbonate co-precipitation of Gd_2O_3-doped CeO_2 solid solution nano-particles, Mater. Sci. Eng. A 383 (2004) 229–234.
[12] M. Sommer, W.D. Schubert, E. Zobetz, P. Warbichler, On the formation of very large WC crystals during sintering of ultrafine WC–Co alloys, Int. J. Refract. Met. Hard Mater. 20 (2002) 41–50.
[13] H.C. Kim, I.K. Jeong, I.J. Shon, I.Y. Ko, J.M. Doh, Fabrication of WC–8 wt.% Co hard materials by two rapid sintering processes, Int. J. Refract. Met. Hard Mater. 25 (2007) 336–340.
[14] T.S. Zhang, J. Ma, Y.J. Leng, S.H. Chan, P. Hing, J.A. Kilner, Effect of transition metal oxides on densification and electrical properties of Si-containing $Ce_{0.8}Gd_{0.2}O_{2-\delta}$ ceramics, Solid State Ionics 168 (2004) 187–195.
[15] C. Kleinlogel, L.J. Gauckler, Sintering and properties of nanosized ceria solid solutions, Solid State Ionics 135 (2000) 567–573.
[16] F.L. Zhang, C.Y. Wang, M. Zhu, Nanostructured WC/Co composite powder prepared by high energy ball milling, Scripta Mater. 49 (2003) 1123–1128.
[17] P.L. Chen, I.W. Chen, Grain growth in CeO_2: dopant effects, defect mechanism, and solute drag, J. Am. Ceram. Soc. 79 (1996) 1793–1800.
[18] D.Y. Oh, H.C. Kim, J.K. Yoon, I.J. Shon, One step synthesis of dense $MoSi_2$–SiC composite by high-frequency induction heated combustion and its mechanical properties, J. Alloys Compd. 395 (2005) 174–180.
[19] N. Koichi, Evaluation of K_{IC} of brittle solids by the indentation method with low crack-to-indent ratios, J. Mater. Sci. Lett. 1 (1982) 13–16.
[20] M.C. Martin, M.L. Mecartney, Grain boundary ionic conductivity of yttrium stabilized zirconia as a function of silica content and grain size, Solid State Ionics 161 (2003) 67–79.
[21] M. Aoki, Y.M. Chiang, I. Kosacki, J.R. Lee, H. Tuller, Y. Liu, Solute segregation and grain-boundary impedance in high-purity stabilized zirconia, J. Am. Ceram. Soc. 79 (1996) 1169–1180.
[22] X. Guo, Size dependent grain-boundary conductivity in doped zirconia, Comp. Mater. Sci. 20 (2001) 168–176.